Nuclear Instruments and Methods in Physics Research A321 (1992) 589–597
North-Holland

NUCLEAR
INSTRUMENTS
& METHODS
IN PHYSICS
RESEARCH
Section A

Calculations of the photon dose behind concrete shielding of high energy proton accelerators

D. Dworak * and K. Tesch
Deutsches Elektronen-Synchrotron DESY, Notkestr. 85, D-2000 Hamburg 52, Germany

J.M. Zazula *
CERN, CH-1211 Geneve 23, Switzerland

Received 12 March 1992 and in revised form 25 May 1992

The photon dose per primary beam proton behind lateral concrete shieldings was calculated by using an extension of the Monte Carlo particle shower code FLUKA. The following photon-producing processes were taken into account: capture of thermal neutrons, deexcitation of nuclei after nuclear evaporation, inelastic neutron scattering and nuclear reactions below 140 MeV, as well as photons from electromagnetic cascades. The obtained ratio of the photon dose to the neutron dose equivalent varies from 8% to 20% and it well compares with measurements performed recently at DESY giving a mean ratio of 13%.

1. Introduction

The neutron dose equivalent behind the concrete or iron shield of high energy proton accelerators was calculated recently [1–4]. The well-known Monte Carlo code FLUKA [5] was used which had originally been written to simulate the development of the hadronic cascades in extended materials. The histories of the most important cascade particles are scored until their energies fall below a cut-off energy which is usually 50 MeV for hadrons. Since the larger part of the neutron dose behind a shield is due to neutrons below that energy the original code was extended by linking the original FLUKA code and other modules into one program to describe also the production of low energy neutrons by evaporation and the transport of neutrons with energies down to thermal energy. The resulting neutron dose equivalent is in agreement with experimental data taken behind lateral concrete shields, and calculated neutron spectra agree with spectra measured recently at 7 GeV beam energy [6].

Measurements around all high energy accelerators show that not only neutrons but also photons contribute to the total dose behind a concrete shield. Unfortunately no calculations or systematic estimations of the photon dose at high primary energies exist up to now. The first calculations of photon doses for the case of monoenergetic neutrons impinging on a concrete shield were performed at ORNL [7,8]. The mainly contributing photon production processes, capture of thermal neutrons and neutron interactions below 15 MeV, were taken into account, and the ratio of photon dose to neutron dose was found to be a few per cent for primary neutron energies between 75 and 400 MeV. Measurements of photon spectra behind the shield of a 50-MeV proton accelerator together with some theoretical calculations are published in refs. [9–11].

It was already pointed out in ref. [4] that the problem of calculating photon doses can be solved in the same way as for neutron doses: by further extension of the FLUKA code by modules describing production and transport of photons linked into one program system. For this procedure we consider in the next section all contributing photon production processes which occur in an extended iron target and in a concrete shield, and also the photon transport, input data and some other details. Section 3 presents the resulting photon doses as a function of the lateral concrete thickness for some values of the following parameters: primary energy, diameter of iron target and type of concrete. Photon spectra are shown for some cases. The ratio photon dose to neutron dose equivalent is compared with measurements.

* On leave of absence from the Institute of Nuclear Physics, Krakow, Poland.

2. Input data and calculational details

2.1. General remarks

In order to calculate photon doses behind a concrete shield we considered the following photon-producing processes:

1) Photon production as a consequence of the development of the electromagnetic cascades initiated by high energy photons from the π^0 decay and by electrons and positrons from the decay of muons;

2) Deexcitation of nuclei after evaporation of massive particles;

3) Radiative capture of thermal neutrons;

4) Inelastic interactions of neutrons below 20 MeV and in the range 20–140 MeV.

The first-mentioned processes occur mainly in a target, therefore the photon dose is expected to depend on the target size and on the shield thickness. The three others are mainly processes in the concrete shield, and some sort of equilibrium between the neutron and the photon dose can be expected. For the transport of photons the Monte Carlo code EGS4 [12] was used, which had already been linked as a FLUKA module [5]. Fig. 1 shows the block diagram of our code as far as the extensions of FLUKA handling photons and low energy neutrons are concerned.

Our standard geometry is nearly the same as in our earlier papers and is displayed in fig. 2. The iron target is 2 m long, its diameter is varied as well as shield thickness and material. Neutron fluences were calculated behind the lateral shield; no energy cut for the neutron transport was applied in the innermost parts of the concrete as described earlier [1].

Photon doses were calculated in two different ways as we did for calculating neutron doses in ref. [1]. First, we calculated the absorbed dose in the innermost 2 cm layer (see fig. 2) of a tissue-equivalent material. Second, the fluence of photons entering the 2-cm tissue layer was calculated and multiplied by the fluence-to-dose conversion factors taken from ref. [13]. Both magnitudes should be approximately equal, though the conversion factors are defined for a somewhat different geometry; we used their comparison as an important check of consistency of the used data and method of calculation. In calculating neutron doses by means of conversion factors we used the magnitude current (number of neutrons per unit area of traversed shield boundary) for reasons explained in ref. [3]. To obtain photon doses the magnitude fluence (number of photons per unit area traversing a given boundary, divided by the cosine of their angle between their direction of flight and normal to boundary) is a better approximation. The photon absorption in tissue is a volume-de-

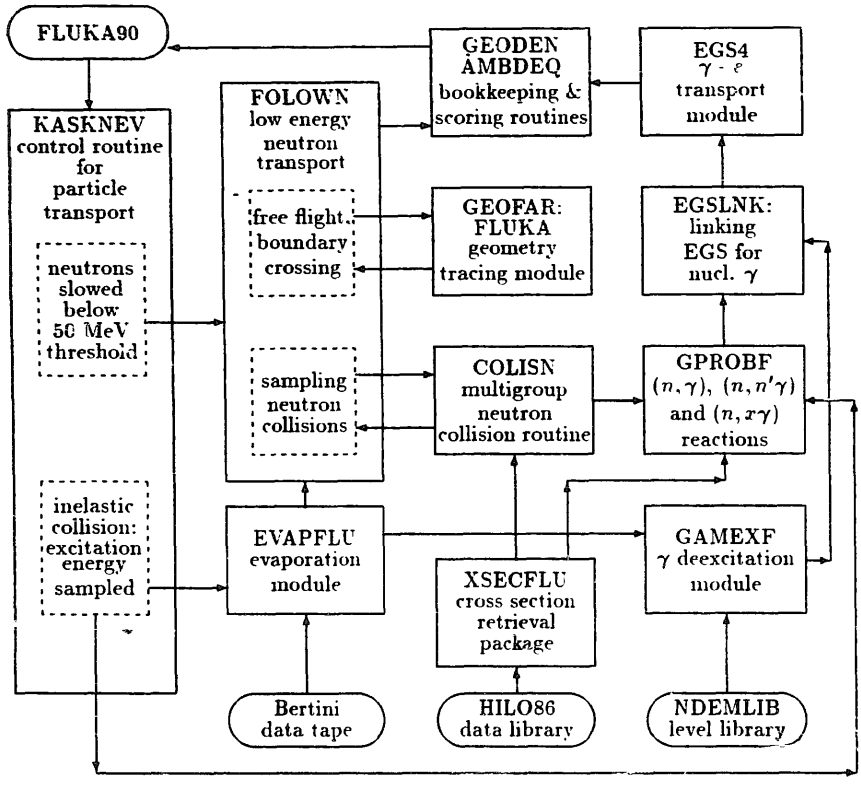

Fig. 1. Simplified flow diagram for sampling of low energy neutrons and photons of nuclear origin in the FLUNEV code.

pendent effect; the attenuation factor for a 2 cm layer is 0.95 and for 30 cm it is 0.47, in the energy range 0.1–10 MeV. By using photon fluence we obtained good agreement between the dose calculated by means of conversion factors and the energy deposited per unit mass in the 2 cm layer of tissue, their mean ratio was 1.20 with a standard deviation of 0.11. One should note here that the statistical accuracy of scoring the absorbed dose is much worse than that of scoring the fluence because only a small amount of energy is deposited in the 2 cm tissue layer. The ratio of dose calculated by current to dose calculated by fluence turned out to be around 0.55 (0.5 is expected for an isotropic source near boundary).

Incorporating the photon production and transport processes mentioned above and estimating their doses increased the simulation time of our code per one primary particle (so far extended to consider low energy neutrons) by a factor of 2.4 (for the geometry of fig. 2 and a 2 cm target diameter). For the runs of the program providing the final results we spent not less than 120 min of CPU time on an IBM 9021.

2.2. *Photons from electromagnetic cascades*

Photons of high energies which create electromagnetic cascades are mainly produced by the decay of π^0 mesons in the target. The number of π^0's depends on the target dimension. It increases from 10 for the geometry shown in fig. 2 with target diameter 0.2 cm to 42 for a 10 cm diameter target, per one 100-GeV proton. A second source of minor importance are electrons and positrons from decaying muons created by charged pions. The calculations show that most of the contributing charged pions come to rest in the iron target or in a 1 m concrete shield, so the initial muon energy is 4.2 MeV. The number of decaying pions increases from about 4 with a thin target (0.2 cm) to 29 with a thick target (10 cm) and determines the number of decaying muons. The spectrum of the finally produced electrons and positrons has its strong maximum near 52 MeV (maximum possible energy of e^+ or e^- from decay of muon in rest), these particles also produce penetrating e–γ-showers. The photon dose outside a 1 m concrete shield initiated by π^0's turns out to be a factor of ten higher than that from the charged pion decays. Although the number of all these elementary processes increases with target thickness, low-energy photons from the cascade are, on the other hand, strongly attenuated in a thicker target, therefore a certain target thickness is expected that produces a maximum dose outside a given shield.

The development of the electromagnetic cascade was calculated by the EGS4 module [12]. Each time a photon, electron or positron is created by FLUKA, EGS is called, and the particles are transported through the system until they are absorbed, escape from the system, or are slowed down below an energy threshold. We used a threshold of 1 MeV for electrons and positrons and 10 keV for photons. The program provides the use of leading particle biasing in user-specified geometry regions; we used this option for processes inside the target and the concrete shield.

With the available standard version of the EGS program the photon dose outside the concrete shield is easily determined by calculating the energy deposition in the 2-cm layer of tissue. Unfortunately the statistical accuracy of this calculation is low because only a small amount of energy is lost in such a layer. We therefore added a procedure to score all photons entering this layer and to calculate their dose by means of fluence-to-dose conversion factors. We found good agreement between the results of both methods when using very long-running computer jobs with high accuracy, their mean ratio is 1.08 with a standard deviation of 0.21. Furthermore, the procedure enables the user to calculate the spectrum of photons crossing given boundaries.

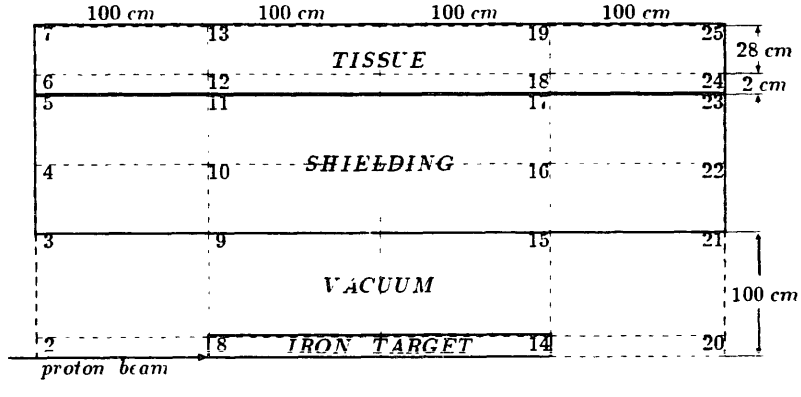

Fig. 2. Cylindrical geometry model of the shielding arrangement assumed for calculations. Solid lines are material boundaries, dashed lines are region boundaries, region numbers are indicated in top right or left corners.

2.3. Photons from deexcitation of nuclei

Photons from further deexcitation of nuclei following evaporation of massive particles are sampled by interfacing the NDEM module of the HERMES code system [14]. For a nucleus of given atomic and mass numbers and residual excitation energy, data such as nuclear levels, shell and pairing energy are available. However, only the lowest option of the physical models of NDEM were used, assuming no discrete line photon spectrum but a continuum of nuclear states. In this manner the use of the module is made as simple and fast as possible, and the amount of required data is substantially reduced. The number and energies of emitted photons are sampled and transferred back to FLUKA where photon directions are selected isotropically. Next, the EGS program is called to transport each photon.

The described assumptions are so crude that the display of a calculated photon spectrum would be meaningless. Nevertheless we believe that estimates of integral magnitudes, like a photon dose, are sufficiently accurate to determine the contribution of the deexcitation processes to the total dose.

2.4. Photons from capture of thermal neutrons

In calculating neutron doses the treatment of thermal neutrons can be performed in simplified manner because their contribution to the total dose is very small. In ref. [1] we assumed a thermal neutron to be absorbed within one diffusion length. For our present problem we calculated the distribution of thermal neutrons more accurately since photons from neutron capture turned out to be the largest contribution to the photon dose. When a neutron reaches the thermal energy group (below 0.414 eV) it is transported in an analog way without changing its weight until it is absorbed or is escaping the system (the non-analog absorption, i.e. multiplication of the neutron weight by the nonabsorption probability, is the usual biasing option used in the neutron transport module adopted from the MORSE code [15]). Capture of thermal neutrons is sampled using the ratio of absorption to total cross sections. The weight of the produced photon is the product of the thermal neutron weight, the ratio of photon production cross section to neutron absorption cross section, and the γ-ray multiplicity. Its direction of flight is selected isotropically, the transport is calculated by the EGS program.

The calculations show that the main contribution to the number of produced capture photons in concrete is from silicon (33%), followed by hydrogen (26%) and iron, sodium and calcium (36% together).

2.5. Photons from inelastic neutron collisions

Another source of photons are inelastic scattering and reactions of neutrons with energies up to about 100 MeV. The calculation of this contribution is not simple and suffers from inconsistencies of data below 20 MeV and lack of data above this value. It would be possible to use the HILO86 multigroup library data [16] based on the compilation ENDF/B-V for calculating the photoproduction, however, the total photoproduction cross sections of this library are not in good agreement with data from another library, the ENDL data set [17], and the upper limit of both packages regarding photoproduction is 20 MeV only. To estimate the contribution of higher energy neutrons, we used the photon production cross sections for protons measured by Zobel et al. [18] between 15 and 150 MeV, assuming that the corresponding cross sections due to neutrons of the same energy are not too differ-

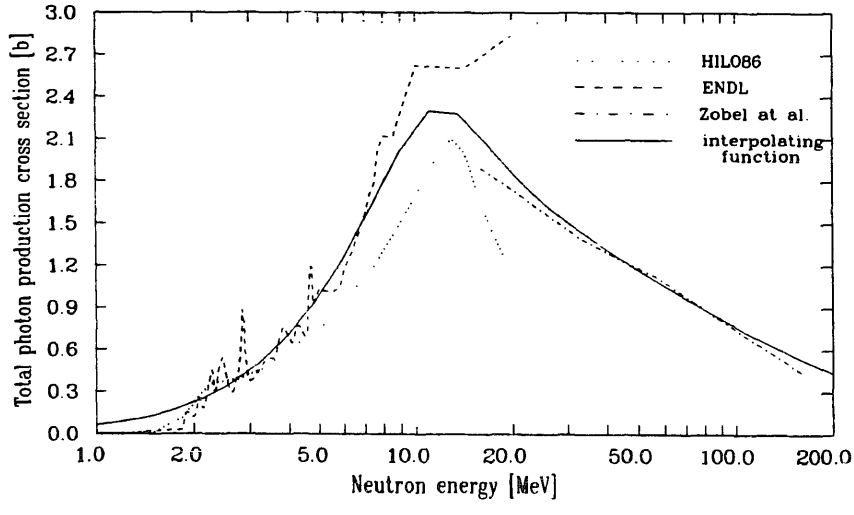

Fig. 3. Total photon production cross section for silicon from three data sources and an interpolating function.

ent. At 20 MeV the absolute values of the proton cross sections match quite well with the neutron data of the two libraries mentioned before, for all nuclei of a concrete shield. As an example, fig. 3 shows the total photon production cross sections derived from HILO86 and from ENDL and the data of Zobel et al. for silicon. The solid line is an interpolated analytic function. Such a curve was calculated for each element (except hydrogen) of each medium of the system and used in the calculations at neutron energies above 2–5 MeV; below these energies as well as for hydrogen the HILO86 total photoproduction cross section were used. The HILO86 total neutron cross-section data are used in the whole energy range to receive the photon production probability for a particular neutron group that is obtained as the ratio of the photon production cross section to the total neutron cross section.

Since the two libraries provide no data on the spectrum of photons produced by neutrons above 20 MeV we assumed that their relative energy distribution is the same as that induced by neutrons in the highest energy group of HILO86, 17.5 to 19.6 MeV. This rather unphysical assumption is too crude to calculate a reliable photon spectrum for high neutron energies; nevertheless we believe that the calculation of an integral magnitude like dose from such a spectrum is good enough to demonstrate the relatively small contribution of high energy neutrons to the total photon dose.

Emitted photons are sampled after each neutron collision. The number of generated photons equals the integer part of the photon yield; Russian roulette is played for emission of an additional photon corresponding to the fractional part of it. The weight of each photon is the same as the weight of the neutron before collision.

2.6. Neglected photon-producing reactions

The photon production by protons (and other charged particles) can be neglected. As an example, the total (p, $x\gamma$) cross section of silicon is around 1 b in the energy range 10–100 MeV [18] which gives a mean free path λ in concrete (34% silicon by weight) of 57 cm for this reaction. The range R of protons in concrete is 4.2 cm at 100 MeV and 0.24 cm at 20 MeV, so R/λ is much smaller than 1.

The direct production of photons by n–p collisions inside the nucleus is also negligible. This process gives a photon spectrum which was measured from 20 MeV up to beam energy and found to be exponentially decreasing like bremsstrahlung [19]. However, the cross section for this reaction is small. The ratio of the cross section to the total neutron reaction cross section can be estimated from the data given in ref. [19], section 3.1, and is roughly 0.001.

3. Results

In table 1 we display the number of photons produced in reactions with the nuclei of concrete to demonstrate the relative importance of the various processes described in the preceding section. The data are given per one primary proton of energy 100 GeV, and they concern the geometry shown in fig. 2, with two target diameters and the shield thickness 1 m. Around half of the emitted photons are from capture of thermal neutrons, the smallest contribution is due to interactions of neutrons in the range 50 to 140 MeV. Fig. 4 shows the calculated photon spectrum from capture of thermal neutrons in concrete as an example.

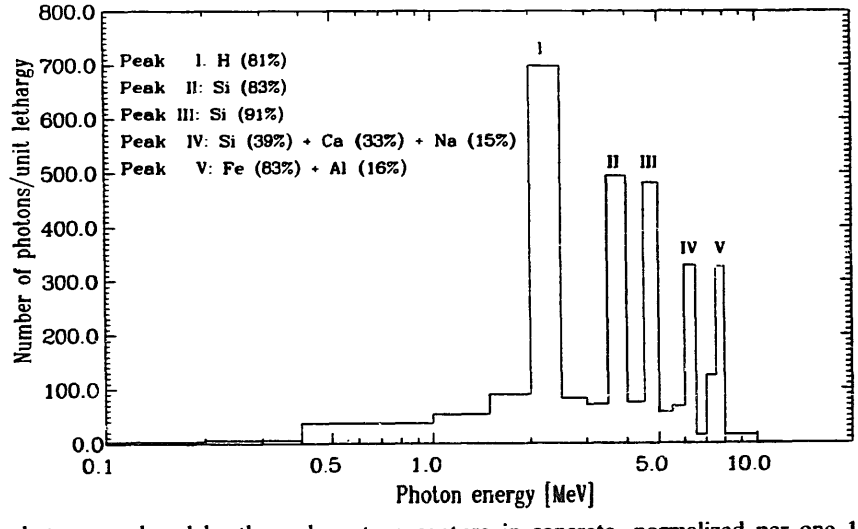

Fig. 4. Spectrum of photons produced by thermal neutron capture in concrete, normalized per one 100-GeV proton. Target diameter 2 cm.

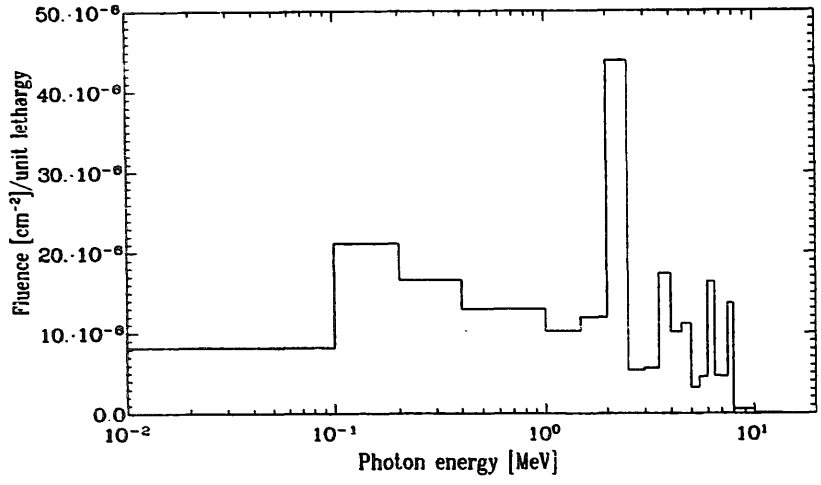

Fig. 5. Fluence of photons from capture of thermal neutrons and inelastic interactions below 20 MeV entering the 2-cm tissue layer behind a 1 m concrete shield, per cm^2 and per one 100-GeV proton, averaged over regions 12, 18, and 24. Target diameter 2 cm.

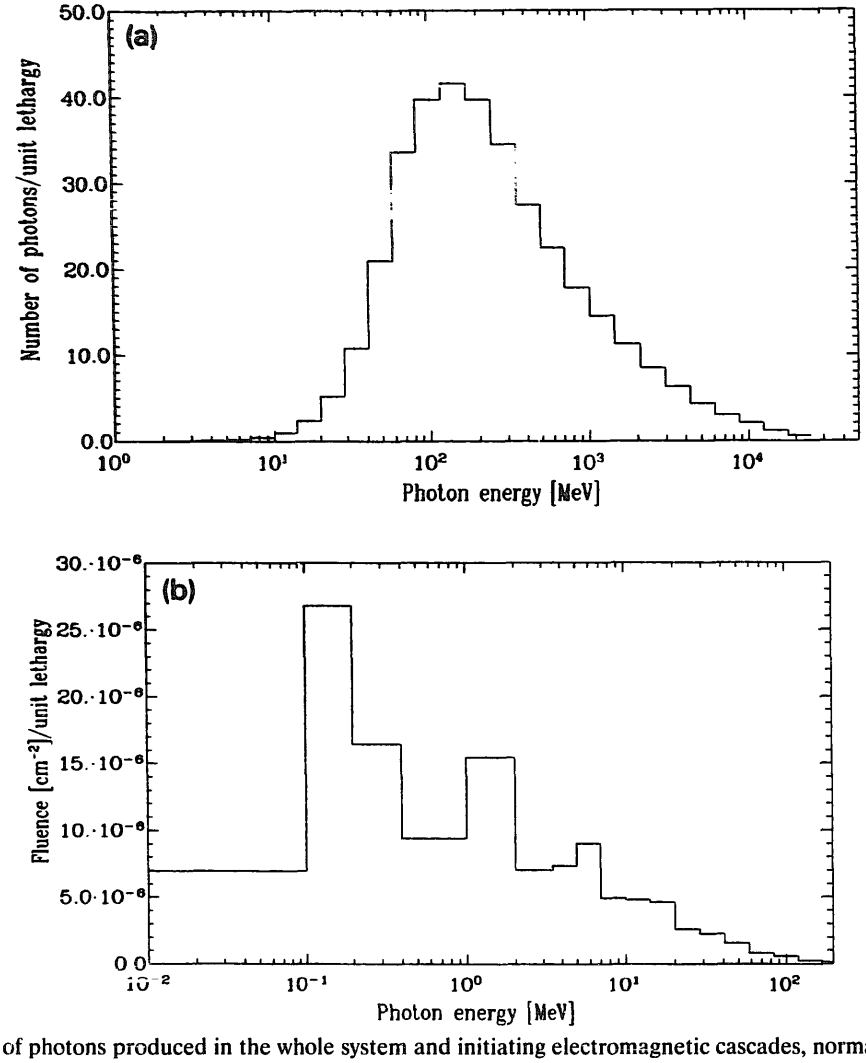

Fig. 6. (a) Spectrum of photons produced in the whole system and initiating electromagnetic cascades, normalized per one 100-GeV proton. (b) Fluence of cascade photons entering the 2-cm tissue layer behind a 1 m concrete shield, per cm^2 and per one 100-GeV proton, averaged over regions 12, 18, and 24. Target diameter 2 cm.

Table 1
Number N_γ of photons of nuclear origin emitted in the 1 m thick lateral concrete shield for two diameters of iron target, per one 100-GeV proton

Origin	N_γ	
	10 cm diam.	2 cm diam.
Thermal neutron capture	465 (55%)	216 (44%)
Deexcitation of nuclei	60 (7%)	48 (10%)
Inel. neutron scatt. and react.:		
E_n = 0.414 eV–20 MeV	218 (26%)	146 (30%)
20–50 MeV	96 (11%)	69 (14%)
50–140 MeV	12 (1%)	9 (2%)
Total	851 (100%)	488 (100%)

Table 2
Photon doses H_γ from various photon sources in the whole system, behind 1 m lateral concrete shielding and for the 2 cm iron target diameter, per one 100-GeV proton. 1.4–16 means 1.4×10^{-16}

Origin:	H_γ [Sv]
Thermal neutron capture	1.4–16 (21%)
Deexcitation of nuclei	5.0–17 (7.4%)
Inel. neutron scatt. and react.:	
E_n = 0.414 eV–20 MeV	4.2–17 (6.4%)
20–50 MeV	3.3–17 (4.9%)
50–140 MeV	7.3–18 (1.1%)
All nuclear photons	2.7–16 (41%)
Electromagnetic cascade	4.0–16 (59%)
Total	6.7–16 (100%)

The data are given as number of photons per unit of logarithmic energy interval. The peaks can be attributed to several elements. The spectrum of photons produced in the two most important nuclear reactions (capture of thermal neutrons and inelastic interactions below 20 MeV) and entering the 2-cm tissue layer behind a 1 m thick concrete shield is shown in fig. 5. The peaks correspond to those of fig. 4, photons from inelastic reactions show a rather smooth spectrum according to the accuracy of the HILO library. The photons below 0.5 MeV are due to Compton scattering.

In addition to photons of nuclear origin the photons from electromagnetic cascades appear. Their spectrum is presented in fig. 6 (top); it ranges from 10 MeV to 10 GeV. These high energies are drastically reduced by interactions in the sideways concrete shield, the corresponding spectrum is shown in bottom of fig. 6.

Results on photon doses in tissue outside the shield, longitudinally averaged between 1 and 4 m, are shown in table 2. It gives photon doses due to photons of nuclear origin together with the dose from the electromagnetic cascades, for our standard geometry with 1 m concrete and 2 cm target thickness, and per one 100-GeV proton. The most important nuclear process is capture of thermal neutrons, followed by inelastic neutron interactions below 50 MeV and deexcitation of nuclei.

A dependence of the photon dose on the shape of the target is demonstrated in table 3 for two primary energies; its dependence on shielding thickness is shown in its lower part. Behind a concrete thickness larger than 2 m the photon dose due to electromagnetic cascades is negligible; with this thickness the upper end of the photon spectrum is around 10 MeV. One sees also that the ratio of dose due to nuclear photons to neutron dose is about 8% independent of the geometry; an equilibrium between the photon dose and the neutron dose equivalent is reached in a concrete shield of thickness 1 m and more.

Table 3
Photon doses H_γ, neutron doses H_n, and their ratios as a function of primary energy, target diameter and concrete thickness, per one 100-GeV beam proton

E_p [GeV]	Concrete thickness [m]	Target diam. [cm]	H_γs [Sv]		H_n [Sv]	H_γ^{nucl}/H_n [%]	H_γ^{tot}/H_n [%]
			Nucl. photons	e.-m. cascade			
10	1	0.2	2.7–17	3.3–17	3.0–16	8.9	19.6
10	1	2.0	4.4–17	5.2–17	5.1–16	8.5	18.8
10	1	5.0	5.1–17	5.0–17	6.0–16	8.5	16.8
10	1	10.0	5.7–17	4.9–17	6.5–16	8.7	16.2
100	1	0.2	9.4–17	1.2–16	1.1–15	8.2	19.0
100	1	2.0	2.7–16	4.0–16	3.2–15	8.6	21.1
100	1	5.0	3.6–16	4.5–16	4.0–15	9.0	20.4
100	1	10.0	3.8–16	3.5–16	4.4–15	8.6	16.6
100	1.5	10.0	5.7–17	2.4–17	7.8–16	7.3	10.4
100	2.0	10.0	1.3–17	4.4–18	1.8–16	7.4	9.8
100	2.5	10.0	3.2–18	9.0–20	3.3–17	9.6	9.9

Table 4 gives the two photon dose components, the neutron dose and their ratios for several shieldings, 100 GeV proton energy, and for the target diameter of 2 cm which may simulate the glancing incidence of a beam on a parallel object like a magnet. The ratio of the total photon dose to the neutron dose is about 8% again except behind thin shields where it varies between 10 to 20%, due to the contribution from the electromagnetic cascades, and except a sand shield (18 to 22%), because of its higher transparency for photons compared to that for neutrons.

The absolute values of photon doses cannot be compared with measurements since a shielding experiments with a well-defined source and simple geometry was nowhere performed. Instead we determined the ratio of photon dose to neutron dose equivalent in several locations around our proton synchrotron (7 GeV) and the proton booster PETRA (7–40 GeV). The neutron spectroscopy and dosimetry is described in ref. [6]. Photon doses were measured simultaneously by means of ^{7}LiF thermoluminescent dosemeters. The neutron sensitivity of ^{7}LiF relative to its photon sensitivity is low, its neutron response was calculated [20] and measured [21] and it covers the range 0.001–0.01 Gy/Sv for the neutrons of energy between 0.01 and 20 MeV. For the neutrons up to 100 MeV this value will not become much larger since the cross sections for elastic and inelastic scattering of neutrons and for nuclear reactions with ^{7}Li and F are decreasing whereas the fluence-to-dose conversion factors remain approximately constant. Other particles which could contribute to the dose measured in ^{7}LiF are high energy protons and charged pions. We calculated the ratio of the dose from these particles to the total neutron dose equivalent and received a value of less than 0.02 behind 1 m of concrete. The contribution of muons from pion decay is also very low; the corresponding ratio turned out to be less than 0.01. Though these numbers suffer from poor statistical accuracy they lead us to the conclusion that more than 80% of the measured ^{7}LiF dose is due to photons of nuclear origin and from electromagnetic cascades.

We measured the ratio of the dose in ^{7}LiF to the total neutron dose equivalent in 14 locations behind existing shieldings of ordinary concrete, heavy iron-loaded concrete ($\rho = 3.7$ g/cm^3), sand and combinations of these materials; the concrete shields were between 0.8 and 2 m, the sand about 3 m. A mean ratio of 0.16 was found with a standard deviation of 0.03 [6], thus a pure photon dose is about 13% of the neutron dose. This result is in agreement with the experience gained at other accelerators and supports our theoretical calculations.

References

[1] J.M. Zazula, K. Tesch, Nucl. Instr. and Meth. A286 (1990) 279.
[2] J.M. Zazula, K. Tesch, Nucl. Instr. and Meth. A300 (1991) 164.
[3] K. Tesch, J.M. Zazula, Nucl. Instr. and Meth. A300 (1991) 179.
[4] J.M. Zazula, Internal Report DESY-D3-69 (1990).
[5] P.A. Aarnio, J. Lindgren, J. Ranft, A. Fassò and G.R. Stevenson, CERN Reports TIS-RP/168 (1986) and TIS-RP/190 (1987).
[6] D. Dinter and K. Tesch, Internal Report DESY-D3-70 (1991) (submitted to Radiation Protection Dosimetry).
[7] R.G. Alsmiller, F.R. Mynatt, J. Barish and W.W. Engle, Nucl. Instr. and Meth. 72 (1969) 213.
[8] R.W. Roussin, R.G. Alsmiller and J. Barish, Nucl. Eng. Design 24 (1973) 250.
[9] Y. Uwamino, T. Nakamura and K. Shin, Nucl. Sci. Eng. 80 (1982) 360.
[10] T. Nakamura, M. Joshida and K. Shin, Nucl. Instr. and Meth. 151 (1978) 493.
[11] K. Shin, K. Hibi, M. Fujii, Y. Uwamino and T. Nakamura, Phys. Rev. C29 (1984) 1307.
[12] W.R. Nelson, H. Hirayama and D.W.O. Rodgers, Stanford Linear Accelerator Center, Report SLAC 265 (1985).
[13] International Committee for Radiation Protection, ICRP Publication No. 51 (1987).

Table 4
Photon doses H_γ, neutron doses H_n, and their ratios for several shieldings, per one 100-GeV proton. Target diameter 2 cm

Shielding		H_γ [Sv]		H_n [Sv]	H_γ^{nucl}/H_n [%]	H_γ^{tot}/H_n [%]
		Nucl. photons	e.-m. cascade			
Ordinary concrete	1.0 m	2.7–16	4.0–16	3.2–15	8.6	21.1
	1.5 m	5.0–17	2.0–17	6.8–16	7.3	10.3
	2.0 m	1.1–17	3.0–18	1.7–16	6.4	8.2
	2.5 m	2.4–18	3.7–19	3.7–17	6.5	7.5
Heavy concrete	0.5 m	1.6–15	1.1–15	1.9–14	8.6	14.3
	1.0 m	1.4–16	1.6–17	1.9–15	7.2	8.0
h.concr. 0.5 m + sand	1.0 m	1.8–16	8.4–17	1.5–15	12.5	18.2
	2.0 m	2.7–17	9.6–18	1.7–16	16.3	22.1

[14] P. Cloth, D. Filges, R.D. Neef, G. Sterzenbach, Ch. Reul, T.W. Armstrong, B.L. Colborn, B. Anders and H. Bruckmann, Kernforschungsanlage Jülich, Report JUL-2203 (1988).
[15] M.B. Emmet, Oak Ridge National Laboratory Report ORNL – 4972 (1975).
[16] R.G. Alsmiller, J.M. Barnes and J.D. Drischler, Nucl. Instr. and Meth. A249 (1986) 455.
[17] D.E. Cullen and P.K. McLaughlin, ENDL-84, IAEA-NDS-11, Rev. 4 (1985).
[18] W. Zobel, F.C. Maienschein, J.H. Todd and G.T. Chapman, Nucl. Sci. Eng. 32 (1968) 392.
[19] H. Nifenecker and J.A. Pinston, Ann. Rev. Nucl. Part. Sci. 40 (1990) 113.
[20] H. Hashikura, K. Haikawa, S. Tanaka and S. Kondo, J. Fac. Eng. Univ. Tokyo (B) 34 (1987) No. 1.
[21] J.A.B. Gibson, Rad. Prot. Dosimetry 15 (1986) 253.